Met. Mater. Int., Vol. 22, No. 3 (2016), pp. 356~363
doi: 10.1007/s12540-015-5158-3

Practical Determination of Friction Coefficient of Al 3003 for Forming of Backward Extruded Part Using Simple Tip Test and Inverse Finite Element Analysis

H. J. Bong[1,#], D. Leem[1], J. H. Kim[2,*], Y. T. Im[3], and M. G Lee[4,*]

[1]Graduate Institute of Ferrous Technology, POSTECH, Pohang, Gyeongbuk 37673, Korea
[2]School of Mechanical Engineering, Pusan National University, Busan 46241, Korea
[3]Department of Mechanical Engineering, KAIST, Daejeon 34141, Korea
[4]Department of Materials Science and Engineering, Korea University, Seoul 02841, Korea

(received date: 26 March 2015 / accepted date: 30 June 2015)

The friction coefficient for aluminum alloy 3003 was determined from a specially designed tip test and finite element (FE) simulations. Measured radial tip distance after the tip test was compared to the FE simulations by iteratively changing friction coefficient and the best fitting friction coefficient was determined. To consider strain rate effect on flow stress response during large plastic deformation, a new combined Hollomon-Voce hardening law was proposed. The friction under three different surface conditions was considered by the proposed inverse FE analysis. The results showed that there was obvious strain rate effect on the predicted punch load in the tip test. Moreover, the different friction coefficients were numerically determined for punch/workpiece and die/workpiece interfaces. Two possible causes of this difference were discussed by the analysis on contact normal pressure and slip velocity distributions of the two interfaces.

Keywords: tip test, computer simulation, metals, strain rate, friction coefficient

1. INTRODUCTION

Aluminum (Al) alloys have been used for numerous industrial applications in the fields of aerospace, automotive, and battery. The Al alloys have good mechanical properties and low density [1]. Of the Al alloys, Al 3003 has gained attention because this alloy has positive strain rate sensitivity (SRS). Therefore, it is better formable than other Al alloys at high forming speed which is beneficial to increase the production speed or to decrease overall cost.

In the metal forming processes, friction between workpiece and forming tool is very important parameter that influences the forming load and the quality of the final product. In addition, the friction determines dimensional accuracy of the complex parts. However, accurate determination of the friction is extremely challenging because it is affected by many factors such as contact area between tool and workpiece, the surface quality of tools, normal contact pressure, tangential slip velocity, environmental conditions such as temperature and humidity, and lubricant.

In the bulk forming applications, there were several approaches to study the frictional behavior. The ring compression test was the most widely applied method owing to its simplicity [2,3]. However, in this method a non-linear calibration must be used to determine the friction coefficient. Moreover, the buckling for large deformation limited the application of the ring compression test. For these reasons, as alternative to the ring compression test, backward extrusion test [4], spike forging [5] and injection upsetting [6] methods were proposed. But, these methods also required a non-linear calibration curve to determine the friction coefficient.

As a new approach, Im *et al*. proposed the so-called tip test based on the backward extrusion [7]. In this method, a radial tip formed at the end of extruded billet was measured [7]. Since this type of method fell in an indirect friction measurement, an inverse approach using FE simulations was often used. The radial tip distance was directly correlated with the friction conditions [8-10]. The numerical investigation of the tip test by Im *et al*. [7] revealed that the friction coefficients were different between interfaces of punch and die. Kang *et al*. [8] investigated the effect of strain hardening on the tip test result. The main advantage of the tip test was that the optimized friction coefficient could be directly associated to the backward extrusion process so that simulation for this process could be more reliable.

In the earlier studies, the strain hardening was simplified and the strain rate effect was not investigated. Also, the discussion on the different friction behaviors in the punch and

*Corresponding author: myounglee@korea.ac.kr, kimjh@pusan.ac.kr
#Present address: Dept. of Materials Science and Engineering, The Ohio State University, Columbus, OH 43210, USA

die interfaces was not properly presented. Considering these limitations, the present study aimed to provide more in-depth analysis of the effect of the SRS of Al 3003 on the friction coefficient. For this, a newly modified Hollomon/Voce hardening law considering the strain rate effect was proposed. In addition, the discussion on possible reasons of different friction coefficients in the two interfaces was provided by the FE simulations. Note that the earlier works on the tip test for the determination of friction behavior used the shear friction factor concept instead of Coulomb's friction coefficient. However, since the main objective of the current work was to study the effect of the material model and to explain the reason of the different friction coefficient in the two interfaces, the Coulomb's friction coefficient commonly used in the metal forming community was employed. In fact, both concepts for the frictional description, i.e., shear friction factor and Coulomb's friction coefficient, have been well accepted for the simulation of bulk metal forming including backward extrusion process [9-11].

2. EXPERIMENTAL PROCEDURE

2.1. Uniaxial test

The mechanical properties of Al 3003 were measured by the uniaxial tension test. The test was carried out in the RB 302 ML™ universal testing machine. Test specimens were prepared according to the ASTM E8 and only the tests along the rolling direction (RD) were conducted. MTS LX 500 laser extensometer was used to measure longitudinal strain. For measuring the SRS of the material, tensile tests under different strain rates were conducted. The strain rates were 0.001, 0.01, 0.1, and 0.3/s at room temperature (RT). At least three tests were repeated for each condition. The test above strain rate of 0.3/s could not be conducted due to the limited capacity of the testing machine. Note that the major deformation mode for the backward extrusion which will be main process method is compression, but the aluminum alloy is known to have symmetric elastic and plastic properties between tension and compression.

2.2. Tip test

The dimensions of the punch, die and workpiece used for the tip test experiment and related FE model are given in [12]. The punch moved downward while the die was static. An initially cylinder shaped workpiece of 10 mm diameter and 5 mm height was prepared. The MTS press machine with a maximum load of 100 kN was used for the experiment. All experiments were conducted at RT. The punch stroke and velocity were 4 mm and 1 mm/s, respectively. To investigate the effect of interface conditions on the frictional behavior, a semisolid type lubricant, grease (G) and phosphate coating, i.e., Bonderite processing (B) were considered. The test was performed for three different lubrication conditions as listed in Table 1 and they were named as 'G/G', 'B/G' and 'B/B'.

Table 1. Condition of lubrication

Interface	G/G	B/G	B/B
P (Punch/workpiece)	Grease	Bonderite	Bonderite
D (Die/workpiece)	Grease	Grease	Bonderite

In the tip test, there are two interfaces, i.e. punch/workpiece and die/workpiece. Hereafter, the interface between the punch and the workpiece and the interface between the die and the workpiece are named as "Interface P" and "Interface D", respectively.

3. FLOW STRESS MODELING IN CONSIDERATION OF STRAIN AND STRAIN RATE

The combined Hollomon-Voce (H/V) model could describe strain hardening characteristics as a function of temperature and strain rate in a practical way [13]. In this model, Hollomon and Voce type hardening models were combined to include softening effect as the plastic deformation proceeds. In particular, in the range of high strain rate the effect of temperature rise by the plastically dissipated heat could be efficiently considered. In this study, the H/V model was further improved to represent the stress-strain response of Al 3003 at various strain rates more accurately.

The H/V model can be written as,

$$f(\varepsilon_P, T) = \alpha(T) H \varepsilon_P^n + (1-\alpha(T)) V (1 - A e^{-B\varepsilon_P}) \tag{1}$$

$$\alpha(T) = \alpha_1 - \alpha_2 (T - T_0) \tag{2}$$

where H, n, V, A, B, α_1 and α_2 are material constants, ε_P is effective plastic strain, T is temperature, and T_0 is reference temperature. The function $\alpha(T)$ ranges $0<\alpha(T)<1$ and decides the dominance of hardening characteristic between Hollomon ($H\varepsilon_p^n$) and Voce ($V(1\text{-}Ae^{-B\varepsilon_p})$) types.

The strain rate effect was further considered in the equation below,

$$\sigma_f = f(\varepsilon_P, T) \times g(\dot{\varepsilon}_P) \tag{3}$$

The function $g(\dot{\varepsilon}_p)$ is related with softening or hardening by the SRS. The widely used Hosford and Caddell's power law model [14] was selected in this study.

$$g(\dot{\varepsilon}_P) = \left(\frac{\dot{\varepsilon}_P}{\dot{\varepsilon}_{P0}} \right)^m \tag{4}$$

where m is the SRS exponent, $\dot{\varepsilon}_P$ is effective plastic strain rate and $\dot{\varepsilon}_{P0}$ is reference effective plastic stain rate.

T_0 in Eq. (1) and $\dot{\varepsilon}_{P0}$ in Eq. (4) were set as RT and 0.001/s, respectively. Inserting $T = T_0$ leads to $\alpha(T) = \alpha_1$. Then, the remaining constants in Eq. (1) could be determined by fitting

Table 2. Material constants in $f(\varepsilon_P, T)$

Constant	Value
H	145.57
V	159.40
n	0.23
A	0.24
B	53.88
α_1	0.64
$R^{2(*)}$ (at T_0 & $\dot{\varepsilon}_{P0}$)	0.9998

*Coefficient of determination

Table 3. SRS exponents, m

Strain rate (/s)	m
0.01	0.0153
0.1	0.0107
0.3	0.0169
Average	0.0143

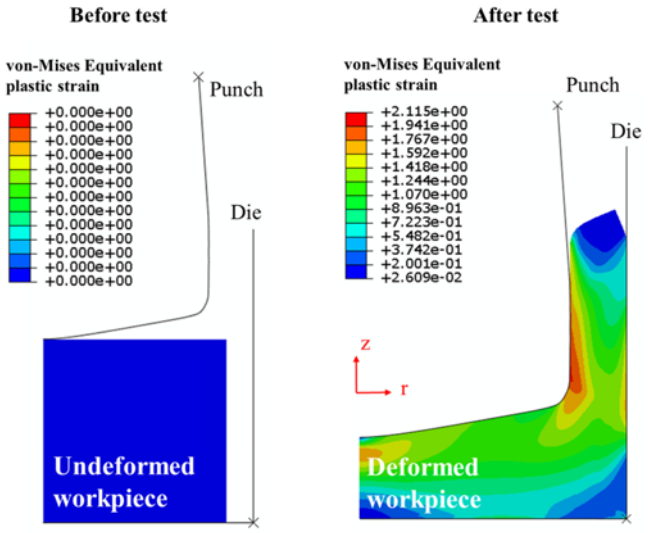

Fig. 1. Finite element models before and after tip tests.

the stress-strain curve at RT and strain rate of 0.001/s. A least square method was applied for the fitting. The determined constants are listed in Table 2. The constant m in Eq. (4) was determined for three stress-strain curves at the strain rate of 0.01, 0.1 and 0.3/s. The determined m values were averaged as listed in Table 3.

4. FINITE ELEMENT MODELING OF TIP TEST

An axisymmetric FE model was used for the simulation of the tip test. This assumption was reasonable because the deformation in this particular test is (almost) axisymmetric. Note that the aluminum alloy exhibited anisotropy in reality, but the earing occurred from this anisotropic nature was simply ignored in the simulation. ABAQUS/Explicit FE code was used to simulate the tip test. The FE model consisted of three components: a punch, a die, and a workpiece. The tools were modeled by an analytical rigid surface and the workpiece was meshed with 4-node axisymmetric solid element with reduced integration (CAX4R). Initial minimum mesh size of 0.015×0.015 mm^2 (length × width) was used. The corresponding 2D FE model is shown in Fig. 1.

The degree of freedom of the die was constrained in all directions, and the punch moved downward by the prescribed displacement boundary condition. The nodes located along the center edge of the workpiece were fixed in the radial (r-) direction, while they could move in the height (z-) direction of the global coordinate system. There were two contact pairs defined in the FE model: (1) the punch and the top surface of the workpiece and (2) the die, and the bottom surface and the side wall of the workpiece. For the frictional behavior, Coulomb's friction law with a constant friction coefficient was assumed for each contact pair; i.e., $\tau = \mu\sigma_n$. Here, τ is the frictional stress, μ is Coulomb's friction coefficient, and σ_n is the normal stress.

The isotropic elastic-plastic law based on von Mises yield function was used for the workpiece. An elastic modulus and Poisson's ratio were 70 GPa and 0.3, respectively. The isotropic hardening was assumed. As a reference stress-strain curve, the H/V stress-strain relation considering the SRS was used for the FE simulation. However, for the validation of the SRS effect on the predicted accuracy (will be discussed in Section 6.1), FE simulation using the H/V model without the SRS was also performed. For the latter case, $g(\dot{\varepsilon}_{P0})$ in Eq. (3) was set as unity.

During the tip test, the deformation of the workpiece is markedly large, which induces large distortion of the FE meshes. To accommodate this large deformation of the FE meshes, a re-meshing technique [15] or Arbitrary Lagrangian-Eulerian (ALE) scheme [16,17] have been utilized. In this study, the ALE scheme implemented in ABAQUS was adopted.

5. RESULTS

5.1. Stress-strain curves modeled by the modified H/V model

Using the material constants in Table 2 and the averaged SRS exponent m, the true stress-strain curves were calculated and compared with measured curves in Fig. 2. The predicted stress-strain curves in the strain range of 0.001 to 0.3/s were in good agreement with the experiments. Although small discrepancy existed in transient region between elastic and plastic, this was expected to have negligible effect on the numerical accuracy considering large deformation in the tip test. The material showed the marked SRS and the flow stress of 0.3/s was approximately 20% larger than that of 0.001/s. From the result, the H/V model was used as a reference stress-strain hardening model to calculate the friction coefficient using the FE analysis inversely.

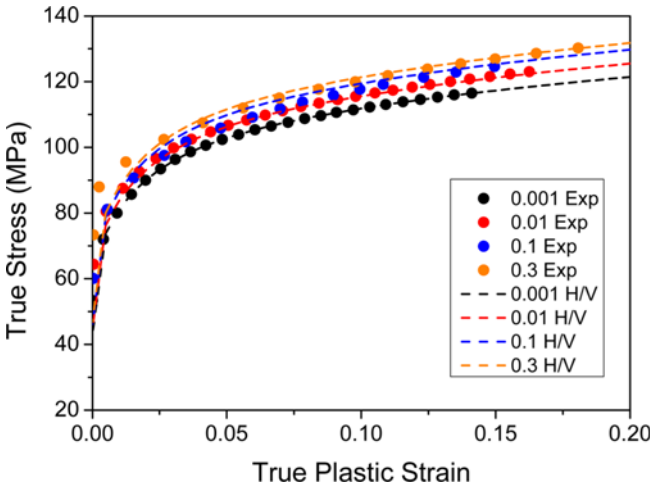

Fig. 2. Stress-strain curves calculated by the modified H/V model and their comparison with measured flow stress curves in the strain rate between 0.001 and 0.3/s.

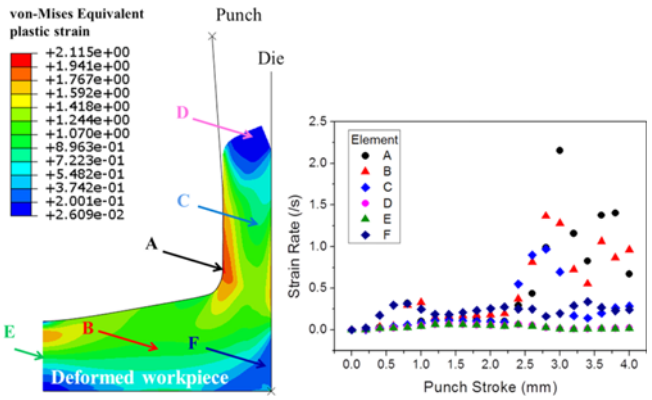

Fig. 3. FE simulated strain rate variation of 6 elements in the workpiece.

The tip test involves very severe plastic deformation or large strain, and the strain rate is non-homogeneous inside the workpiece. From a FE simulated result of the tip test 6 elements at different positions inside the workpiece were selected. Then, the strain rate during the tip test was calculated from the FE simulation result and shown in Fig. 3. The strain rate generally ranges 0~0.3/s, but the strain rate significantly increase up to 2.2/s at certain punch stroke in the element A. The H/V model parameters were determined from strain rate of 0.001 to 0.3/s and the latter is 3000 times faster than the former. The maximum strain rate observed in the FE results, approximately 2.2/s, is only several times faster than strain rate of 0.3/s. Therefore, the modified H/V model is expected to give a reliable prediction of the stress-strain behavior for that high strain rate range.

5.2. Tip test experiment

The radial tip distance was measured after 4 mm punch stroke and the punch load was monitored during the tip test.

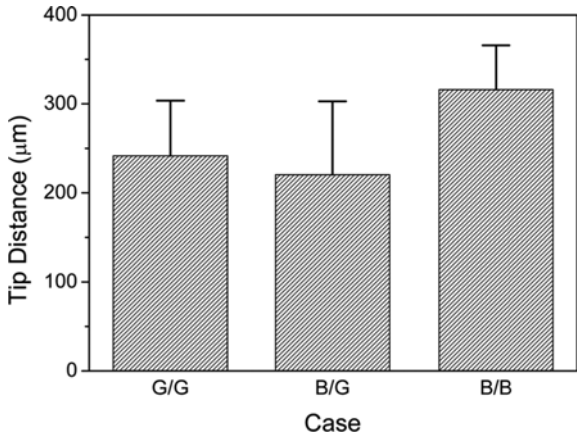

Fig. 4. Radial tip distance after the tip test experiments.

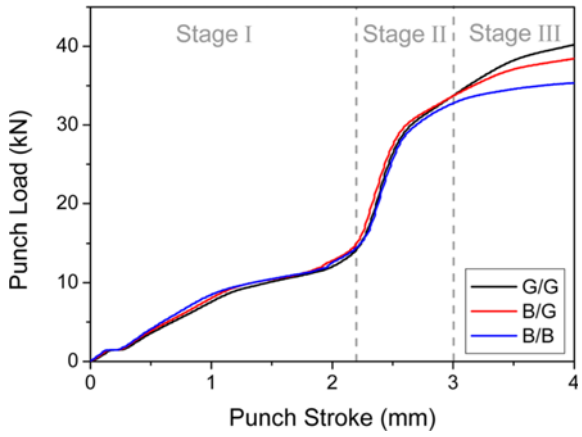

Fig. 5. Punch stroke-load during the tip test experiments.

The measured radial tip distance after the tip test is shown in Fig. 4. The figure shows that the radial tip distance markedly depends on the lubrication, consequently, frictional condition at the interfaces. The largest radial tip distance was measured in B/B.

The punch load-stroke curves during the punch movement of 4 mm in the tip test are shown in Fig. 5. It is notable that the punch loads of the three cases are almost similar until the punch stroke of 2.5 mm. Beyond that stoke, the punch load starts to deviate depending on the lubrication conditions. In the graph, three stages can be observed; i.e., Stage I to Stage III. To observe the deformation aspect during each stage, the tip test was simulated. The variation of the FE simulated workpiece shape during each stage is shown in Fig. 6(a). Stage I (from punch stroke of 0 to 2.2 mm) is upsetting phase of the process and the workpiece deforms in radial direction with the free movement of the side wall of the workpiece. At the beginning of Stage II, the wall of the workpiece contacts the die and the workpiece is extruded backward. The tip is formed at this stage. The backward extrusion continues during Stage III, and the radial tip distance becomes stable in Stage III as

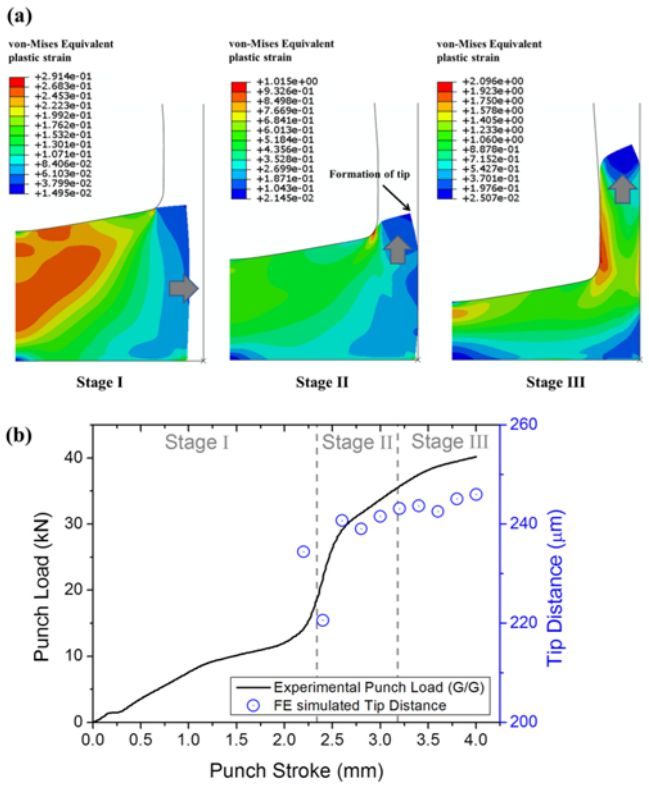

Fig. 6. (a) FE simulated workpiece shape change at each stage (b) Punch stroke-load curve and radial tip distance variation during the tip test (lubrication condition: G/G).

shown in Fig. 6(b) with levelling off the punch load. Note that, to maintain consistency with between experimental and simulation results in Fig. 6(b), determined friction coefficients for G/G were used in the simulation for Fig. 6(b) (The determined friction coefficients will be given in next section).

5.3. Determination of friction coefficient by inverse FE analysis

From the experimental results of the tip test, FE simulations were carried out to determine the optimum friction coefficients that led to the best fittings to the radial tip distance. It was interesting that the objective value; i.e., radial tip distance, could not be well fitted when the same friction constant was used for both punch/workpiece and die/workpiece interfaces. Finally, the best fitting friction coefficients for the three cases are listed in Table 4.

Of the three cases, the friction of B/B is determined as the lowest. Note that the 'B' denotes Bonderite processing, i.e., phosphate coating. The determined friction coefficients show that the friction coefficients at Interface D are always higher than those at Interface P. At Interface D, the same friction coefficient of 0.2 is optimum for both G/G and B/G. However, even with the same semisolid type lubricant, the fitted friction coefficients at Interfaces P and D are quite different; for example, the friction coefficient at Interface P for G/G is 0.07, while that of Interface D for G/G and B/G is almost three times high value of 0.07, i.e., 0.2. This difference in the friction behavior between Interfaces P and D has been observed in earlier works for the same tip tests. In this study, more in-depth analysis will be provided by using the FE analysis to find and suggest possible explanation on this behavior.

Table 4. Determined friction coefficients for the three cases by using inverse FE analysis

Interface	G/G	B/G	B/B
P (μ_1)	0.070	0.055	0.055
D (μ_2)	0.200	0.200	0.090

6. DISCUSSION

6.1. Effect of strain rate sensitivity

In this section, the effect of the SRS of Al 3003 on the current inverse numerical procedure for determining friction coefficient is investigated. For this purpose, FE simulation of tip test was additionally performed with non-SRS model. For the simulation, same friction coefficients, determined with SRS model in Table 4, were used. Then, by comparing the simulated radial tip distance and punch load with the reference data the effect of the SRS could be confirmed. Fig. 7 shows the calculated radial tip distances by simulating the tip test with and without considering the SRS. The figure shows that the calculated radial tip distances with non-SRS model are almost the same as those with SRS model. This result suggests that the effect of the SRS is minor on the radial tip distance, at least in the current particular example.

The punch load-stroke curves were also compared between the FE calculations using the SRS and non-SRS models. Fig. 8(a) and (b) show the calculated curves and their comparisons with experiments. In contrast to the radial tip distance, the difference between the calculated punch load curves by the SRS and non-SRS models is remarkable. In other words, the model by non-SRS model underestimates the punch load

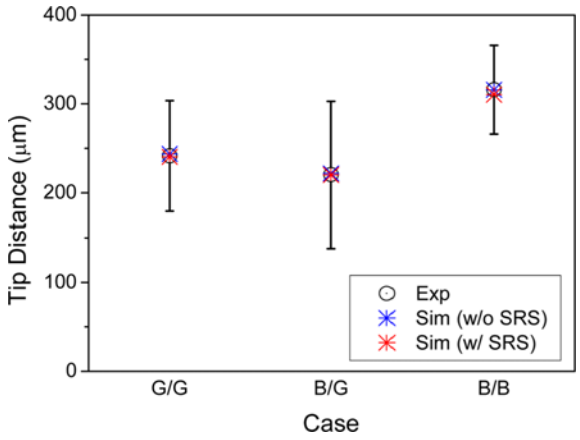

Fig. 7. Radial tip distances calculated by FE simulations using SRS and non-SRS models and their comparison with experimental results.

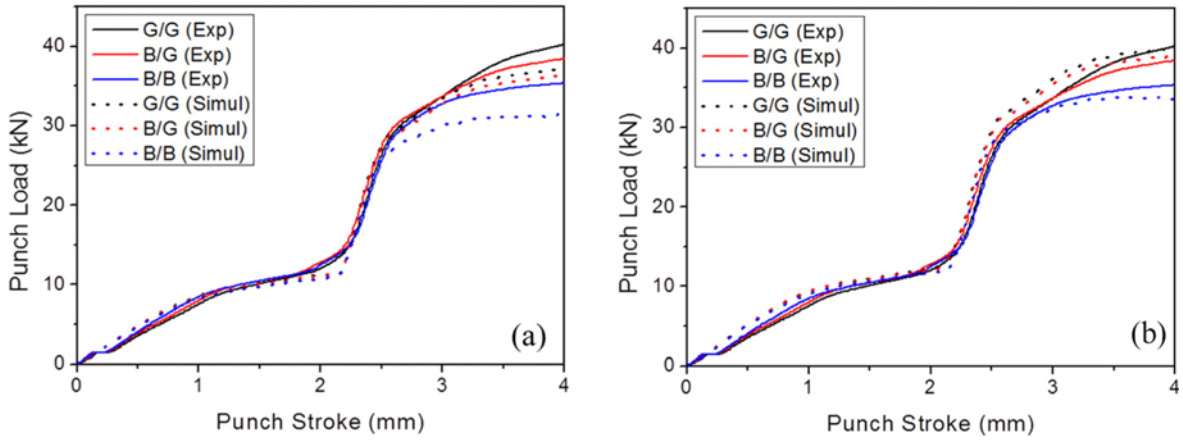

Fig. 8. Experimental and simulation results of punch load-stroke curves during the tip test. (a) Simulation without SRS effect and (b) Simulation with SRS effect.

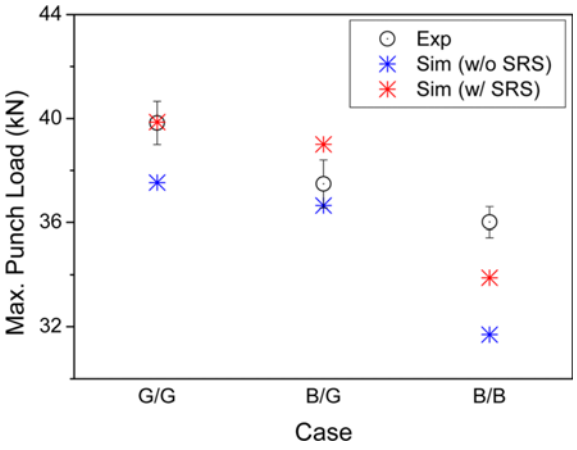

Fig. 9. Experimental and simulation results of the maximum load during the tip test.

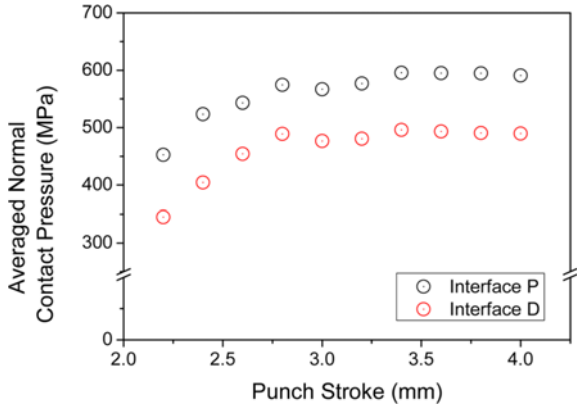

Fig. 10. Variation of the averaged normal contact pressure as a function of the punch stroke.

curves for all three cases. Fig. 9 represents the maximum punch loads during the tip tests for the three lubrication conditions. The simulation results by the SRS and non-SRS models well capture the order of maximum punch stroke, i.e. the maximum punch load is larger in order of G/G, B/G and B/B. However, the simulation by the SRS model leads to better prediction than that by the non-SRS model. Therefore, the results can support the importance of the consideration of the SRS in the tip test.

6.2. Effect of normal contact pressure and tangential slip velocity

A number of factors influence the friction such as normal contact pressure, tangential slip velocity, surface qualities of tools and workpiece, temperature, humidity, and so on. Selected factors among them for this study are the normal contact pressure and the tangential slip velocity to explain the reason for different friction coefficients between Interfaces P and D. This is reasonable because the tool surface, and other environmental conditions like temperature and humidity were similar at the two interfaces. For the analysis, FE simulation can be efficiently utilized assuming that the material behavior is well captured by the modified hardening model.

6.2.1. Normal contact pressure

Normal pressures along the contact interface between tools and workpiece were examined by the FE simulations. To simplify the problem, the friction coefficient was assumed to be the same for both Interfaces P and D; i.e., $\mu_1 = \mu_2 = 0.20$ and the SRS model was used.

The averaged normal contact pressure was calculated based on $\frac{1}{n}\sum_{i=1}^{n} P_i$, where P_i is the normal contact pressure at i^{th} node, and n is the total number of nodes along the interface. In Section 5.2, it was observed that the workpiece (almost) fully contacts with the tool components at the beginning of Stage II, i.e., punch stroke of 2.2 mm. In addition, the required forming load was much more sensitively varied depending on the lubrication conditions. Based on these, Stage II and III were regarded as important stages which determine the frictional behavior. Therefore, the averaged normal contact pres-

sures were calculated for the punch stroke after 2.2 mm.

The variation of the average normal contact pressure as a function of the punch stroke is shown in Fig. 10. The figure reveals that the averaged normal contact pressure at Interface P is always higher than that at Interface D.

6.2.2. Effect of slip velocity

The tangential slip velocity along the contact interface between tool components and workpiece was also examined from the FE simulation. The same friction coefficient and material model as the previous example were used. The averaged tangential slip velocity was obtained from the simple equation, $\frac{1}{n}\sum_{i=1}^{n} v_i$, where v_i is the tangential slip velocity at i^{th} node, and n is the number of nodes along the interface. The variation of the average slip velocity was also considered after the punch stroke of 2.2 mm. The average tangential slip velocity as a function of the punch stroke is shown in Fig. 11. The figure shows that the averaged tangential slip velocity at Interface P is always higher than that at Interface D. In the punch stroke range around 2.6~2.8 mm, backward extruded part of the workpiece (depicted as A, C and D in Fig. 3) deforms faster than other parts. After that, the backward extruded part of the workpiece becomes stable and the radial tip distance becomes stable, consequently, as shown in Fig. 6(b). Due to this, the averaged tangential slip velocity at Interfaces P and D is the highest in that punch stroke range. After that, deformation in the backward extruded part of the workpiece becomes slow and the averaged tangential slip velocity decreases.

6.2.3. Explanation of the difference in friction coefficients at Interfaces P and D

The variations of the friction coefficient as a function of normal contact pressure and tangential slip velocity have been reported experimentally in several earlier studies [18-20]. For example, Azushima and Kudo [19] investigated the dependence of the friction coefficient on the normal contact pressure between a commercial pure aluminum and tools. The decreased friction coefficient was observed as the average contact pressure increased. Chowdhury *et al*. [20] studied the effect of the tangential slip velocity using a rotational friction tester. They found that the friction coefficient decreased with the increase of the tangential slip velocity. Recently, Kim *et al*. [18] investigated the effect of the tangential slip velocity and the normal contact pressure on the friction coefficient for TRIP780 and a mild steel. A newly devised friction tester for high tangential slip velocity and normal contact pressure up to 625 MPa was used. They reported that the decrease of the friction coefficient as the tangential slip velocity and the normal contact pressure increased.

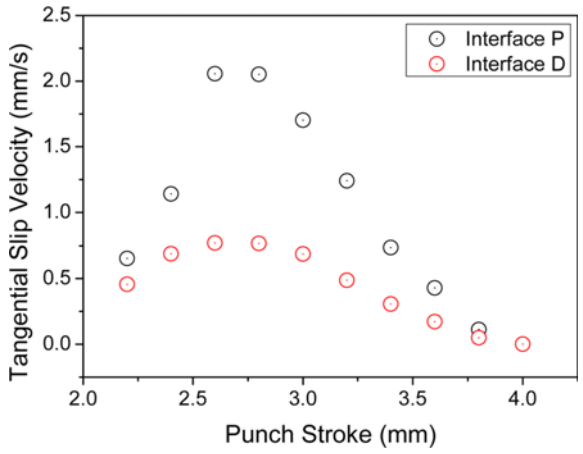

Fig. 11. Calculated averaged tangential slip velocity as a function of the punch stroke.

Although most of the prior researches have been done on sheet metals [21-23], the analysis presented in the current study for a bulk material can be done with the help of the exiting observations. That is, the results in this section show that the tangential slip velocity and the normal contact pressure at Interface P, where determined friction coefficients are smaller, are always higher than those at Interface D. This is well correlated to the conclusion in prior researches. Of course, the normal contact pressure and tangential slip velocity in the current application were not directly measured but calculated by the aid of the numerical modeling. However, in the current method, more accurate hardening model including SRS was introduced and it increased the reliability of the FE simulations. Based on the results in this section, further investigation might be necessary for the analysis on the effect of the two factors to the microscopic condition of surface interface.

6. CONCLUSIONS

The tip test experiments and corresponding finite element (FE) simulations were applied to determine the friction coefficient at the punch and die interfaces for three different lubrication conditions. The radial tip distance was measured from the tip test experiments and the Coulomb's friction coefficient was inversely (and iteratively) determined by comparing it to that calculated from the FE simulation. The summary of the current study and main conclusions are given below.

(1) The flow stress vs. plastic strain relation of Al 3003 could be well captured by the modification of the combined Hollomon-Voce type hardening model, in which the effect of the strain rate sensitivity (SRS) was included. This practical hardening model was implemented in the ABAQUS FE software and used for the FE simulation.

(2) Different friction coefficients were determined at different tool-workpiece interfaces by the suggested inverse approach. The interfaces between punch/workpiece and the die/workpiece have different friction coefficients for all three lubrication conditions. Smaller friction coefficient at the punch/workpiece interface than the die/workpiece was common observation regardless of the lubrication conditions.

(3) The SRS of the Al 3003 in the strain rate range of 0.001 to 0.3/s had minor effect on the radial tip distance when compared with the calculated radial tip distance without the SRS. In contrast, the strain rate effect was more markedly involved in the punch load vs. stroke curve.

(4) The analyses from FE simulations validated that the normal contact pressure and tangential slip velocity at the punch/workpiece interface were always higher than those at the die/workpiece interface.

(5) The smaller friction coefficient at the punch/workpiece interface could be explained by the prior experimental results correlating decreased friction coefficient in the higher normal contact pressure and tangential slip velocity.

ACKNOWLEDGMENTS

This work was supported by the National Research Foundation of Korea (NRF) Grant funded by the Korea government (MSIP) (No.2012R1A5A1048294) and partially by the Korean government R&D programs (Grant No. 10052726) of Ministry of Trade, Industry and Energy. Authors acknowledge H. M. Back and Dr. D. K. Kim at KAIST for their kind helps for the experiments. MGL appreciates support by Korea University Grant.

REFERENCES

1. J. T. Maximov, G. V. Duncheva, A. P. Anchev, and M. D. Ichkova, *Comp. Mater. Sci.* **83**, 381 (2014).
2. H. Sofuoglu and J. Rasty, *Tribol. Int.* **32**, 327 (1999).
3. T. Robinson, H. Ou, and C. G. Armstrong, *J. Mater. Process. Tech.* **153-154**, 54 (2004).
4. T. Nakamura, N. Bay, and Z. L. Zhang, *J. Tribol.-T ASME* **119**, 501 (1997).
5. Y. T. Im, O. Vardan, G. Shen, and T. Altan, *Cirp Ann.-Manuf. Techn.* **37**, 225 (1988).
6. T. Nishimura, T. Sato, and Y. Tada, *J. Mater. Process. Tech.* **53**, 726 (1995).
7. Y.-T. Im, S.-H. Kang, and J.-S. Cheon, *J. Manuf. Sci. E-T. ASME* **125**, 378 (2003).
8. S.-H. Kang, J.-H. Lee, J.-S. Cheon, and Y.-T. Im, *Int. J. Mech. Sci.* **46**, 855 (2004).
9. T. J. Shin, Y. H. Lee, J. T. Yeom, S. H. Chung, S. S. Hong, I. O. Shim, N. K. Park, C. S. Lee, and S. M. Hwang, *Comput. Method. Appl. M.* **194**, 3838 (2005).
10. J. C. Pierret, A. Rassili, G. Vaneetveld, R. Bigot, and J. Lecomte-Beckers, *Int. J. Mater. Form.* **3**, 763 (2010).
11. H. Bašić, I. Demirdžić, and S. Muzaferija, *Int. J. Numer. Meth. Eng.* **62**, 475 (2005).
12. P. Chauviere, K. H. Jung, D. K. Kim, H. C. Lee, S. H. Kang, and Y. T. Im, *J. Mech. Sci. Technol.* **22**, 924 (2008).
13. J. H. Sung, J. H. Kim, and R. H. Wagoner, *Int. J. Plasticity* **26**, 1746 (2010).
14. W. F. Hosford and R. M. Caddel, *Metal Forming: Mechanics and Metallurgy*, pp. 91-92, Prentice-Hall International, Inc. Easnglewood Cliffs, NJ (1983).
15. J.-H. Cheng, *Int. J. Numer. Meth. Eng.* **26**, 1 (1988).
16. W. K. Liu, T. Belytschko, and H. Chang, *Comput. Method. Appl. M.* **58**, 227 (1986).
17. D. J. Benson, *Comput. Method. Appl. M.* **72**, 305 (1989).
18. C. Kim, J.-U. Lee, F. Barlat, and M.-G. Lee, *J. Tribol.-T ASME* **136**, 021606 (2014).
19. A. Azushima and H. Kudo, *Cirp. Ann.-Manuf. Techn.* **44**, 209 (1995).
20. M. Chowdhury, M. Khalil, D. Nuruzzaman, and M. Rahaman, *Int. J. Mech. Mechatron. Eng* **11**, 53 (2011).
21. H. J. Bong, F. Barlat, J. Lee, M. G. Lee, and J. H. Kim, *Met. Mater. Int.* **22**, 276 (2016).
22. G. Cai, L. Lang, K. Liu, S. Alexandrov, D. Zhang, X. Yang, and C. Guo, *Met. Mater. Int.* **21**, 365 (2015).
23. J. C. Jang and S. H. Kim, *Korean J. Met. Mater.* **53**, 618 (2015).